PROCEEDINGS OF SPIE

SPIEDigitalLibrary.org/conference-proceedings-of-spie

Nanoantenna couplers for metal-insulator-metal waveguide interconnects

M. Cengiz Onbasli
Ali K. Okyay

SPIE.

Nanoantenna Couplers for Metal-Insulator-Metal Waveguide Interconnects

M. Cengiz Onbasli[a], Ali K. Okyay*[b,c]
[a]Department of Materials Science and Engineering, Massachusetts Institute of Technology, 77 Massachusetts Avenue, Cambridge, MA 02139, USA
[b]Department of Electrical and Electronics Engineering, Bilkent University, Ankara TR-06800, Turkey
[c]UNAM, National Institute for Materials Science and Nanotechnology, Bilkent University, Ankara TR-06800, Turkey
email: aokyay@ee.bilkent.edu.tr , onbasli@mit.edu

ABSTRACT

State-of-the-art copper interconnects suffer from increasing spatial power dissipation due to chip downscaling and RC delays reducing operation bandwidth. Wide bandwidth, minimized Ohmic loss, deep sub-wavelength confinement and high integration density are key features that make metal-insulator-metal waveguides (MIM) utilizing plasmonic modes attractive for applications in on-chip optical signal processing. Size-mismatch between two fundamental components (micron-size fibers and a few hundred nanometers wide waveguides) demands compact coupling methods for implementation of large scale on-chip optoelectronic device integration. Existing solutions use waveguide tapering, which requires more than 4λ-long taper distances. We demonstrate that nanoantennas can be integrated with MIM for enhancing coupling into MIM plasmonic modes. Two-dimensional finite-difference time domain simulations of antenna-waveguide structures for TE and TM incident plane waves ranging from λ = 1300 to 1600 nm were done. The same MIM (100-nm-wide Ag/100-nm-wide SiO2/100-nm-wide Ag) was used for each case, while antenna dimensions were systematically varied. For nanoantennas disconnected from the MIM; field is strongly confined inside MIM-antenna gap region due to Fabry-Perot resonances. Major fraction of incident energy was not transferred into plasmonic modes. When the nanoantennas are connected to the MIM, stronger coupling is observed and E-field intensity at outer end of core is enhanced more than 70 times.
Keywords: metal-insulator-metal, waveguide, Plasmon resonance, subwavelength, coupler, nanoantenna, dipole

1. INTRODUCTION

Copper interconnects have been the most important medium of signal transfer for complementary metal-oxide semiconductor (CMOS) on-chip and chip-to-chip telecommunications. Copper interconnects have started suffering physical problems such as signal and clock distortion, attenuation, impedance matching, cross-talk, power dissipation per unit area, wave reflection, interconnect density limitations and voltage isolation among multiple devices and components on board[1], as transistor gate lengths have reached below 100 nm regime. Driven by Moore's Law[2], microelectronics industry has provided ingenious solutions to integrate twice as many transistors into the same device area every 18 months. Copper interconnects, however, can no longer follow this trend of even denser packing, because the power dissipation per unit area has started being in the same order of magnitude with sufficient power density dissipation to raise the local temperature of silicon chip substrate to silicon's melting point. That is why; optical waveguides have been introduced as a less-power-dissipating solution. With the appropriate cladding, geometry and sufficient refractive index contrast, optical waveguides can support many different modes and can even serve utilizing wavelength division multiplexing (WDM), not achievable by copper interconnects[1]. Integration density requirements, however, dictate that signal should be transferred by some other means, since waveguides for near-infrared region (780 nm - 3000 nm), need to be larger than ~400 nm in dimensions as can be shown by waveguide theory[3].

Metal-insulator-metal (MIM) waveguides have thus been a major focus of research in the recent years, as it can support (i) wide bandwidth and a range of mode shapes different than higher order waveguide modes, (ii) deep subwavelength capabilities (Our simulations show that penetration depth inside the metal is always below 25 nm, thus structures below

Plasmonics: Metallic Nanostructures and Their Optical Properties VIII, edited by Mark I. Stockman,
Proc. of SPIE Vol. 7757, 77573R · © 2010 SPIE · CCC code: 0277-786X/10/$18 · doi: 10.1117/12.876177

100 nm in width can be used), (iii) CMOS compatibility for fabrication, (iv) the possibility of very high density integration without cross-talk, (v) minimal Ohmic loss, (vi) while still keeping the unique advantages promised by optical waveguiding (WDM)[4]. These features make MIM highly attractive for high sensitivity spectroscopy applications and biosensing[5,6], nonlinear optical phenomena[7,8], waveguiding[9-12], and on-chip signal routing, modulation and processing[13-15]. The disadvantages of MIM are (i) high attenuation per unit length due to inherent losses of the metal claddings at optical and near-infrared bands and (ii) size mismatch with micron-size optical fibers that bring light from optical sources. The first disadvantage is an inherent issue related with material properties used in MIM topology. This disadvantage can however be mitigated to some extent especially in the telecommunication wavelength range (1300 nm and 1550 nm) by analyzing the supported modes of MIM and optimizing MIM waveguide architecture[11,16,17]. The second disadvantage is a significant hindrance against the implementation of large-scale on-chip integration of optoelectronic devices. The size-mismatch between fundamental components for optical clocking, i.e. micron-wide optical fibers and less-than-300 nm-wide MIM, demands a coupler stage for efficient plasmonic mode initiation, otherwise excited plasmonic modes will not propagate more than 10 μm. Long propagation (>20μm) lengths in a deep subwavelength MIM is essential for enabling sufficient versatility to optoelectronic chip designers.

To achieve coupling of incident optical energy from fibers to MIM plasmonic modes, most of the previous solutions focus on the use of a type of a tapered architecture. The proposed tapered architectures require more than 4λ-long taper distances between the fiber's and the MIM's ends, for adiabatic mode transformation from waveguide modes to plasmonic modes[18,19]. To avoid this bulky coupling mechanism, we show that nanoantennas can be integrated with MIM waveguides to achieve (i) enhanced coupling into the MIM waveguide and extended propagation length, and (ii) tune the mode field intensity profile inside the silicon oxide core by changing the antenna length, antenna width and the antenna-waveguide separation. We demonstrate that nanoantennas can be integrated with MIM for enhancing coupling into MIM plasmonic modes. Because nanoantennas are thinner than 150 nm, there is no loss of coupler space as in tapered architectures.

2. THEORY AND SIMULATION

Simulations were done to show that (i) introducing nanoantenna couplers can enhance the coupling into an MIM waveguide while coupling space can be reduced down to less than 200 nm wide antennas, (iii) waveguide output signal can be enhanced significantly (upto more than 70 times) for integration with CMOS compatible nanoscale photodetector elements (i.e. Ge-on-Si photodetectors) placed at the end of the MIM waveguide for conversion of plasmonic signal to pure electrical current. Two and three dimensional finite-difference time domain (FDTD) simulations of antenna-waveguide structures for transverse electric (TE) and transverse magnetic (TM) incident plane waves were done. The incident wavelength has been varied from λ = 1300 to 1600 nm, for on-chip telecommunication applications, where material loss is also smaller with respect to visible. The structures of interest are nanoantenna coupler integrated with the MIM waveguide. The same MIM was used for each different antenna case and the dimensions of the MIM were as follows: 100-nm-wide Ag/100-nm-wide SiO2/100-nm-wide Ag. The antenna consists of a dipole structure of two rectangular silver nanoparticles, whose aspects are submicron. The near-infrared operation wavelength requires submicron aspects of the antennas. Antenna width, length, and antenna-MIM separation distance are varied systematically. The waveguide core width and the distance between antenna arms have been kept equal for each simulated case. The antennas and MIM are assumed to be free-standing in vacuum.

The antenna arm length (longer side) was varied from 50 nm to 700 nm, antenna width (shorter side) was varied between 20 nm and 150 nm and the antenna-waveguide separation has been varied from 0 nm (connected case) to 150 nm. The structures were simulated by varying one dimension at a time, while keeping other dimensions constant. As the reference, the MIM waveguide has been simulated without the antenna, keeping the other conditions the same as in the with-antenna cases. The extinction coefficients for different metals are shown in Fig. 1 as a function of wavelength, following the convention in Palik's handbook[20]. Extinction coefficient (k) is a measure of how fast an electromagnetic wave decays inside the metal and thus is a measure of loss. For achieving long distance plasmonic mode propagation, low k values are sought in the wavelength region of interest (blue region). Silver was chosen as the metal for both antennas and metal claddings of the MIM waveguide for (i) simplicity of analysis, (ii) lower loss with respect to many other metals in the wavelength region of interest, (iii) the high conductivity of silver, since the metal claddings can also be used as contacts for MIM waveguide modulators of plasmonic modes.

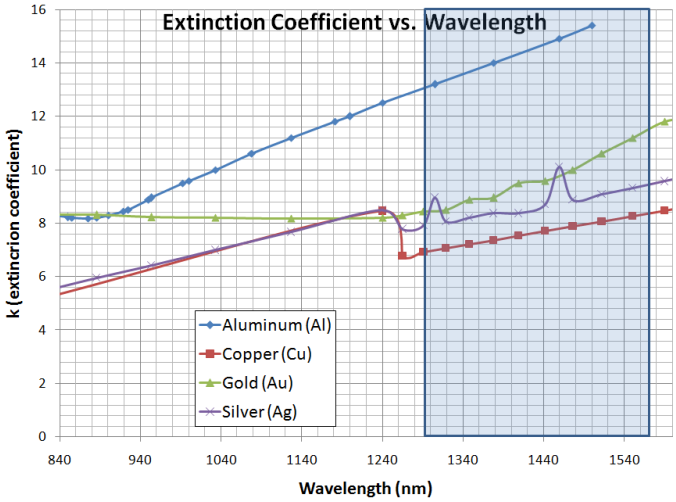

Figure 1. Extinction coefficients for different metals as a function of wavelength as given in Palik's handbook of optical constants.

For geometry definitions and simulations, Lumerical FDTD Solutions™ were used[21]. The structures were divided into rectangular meshes with non-uniform mesh widths and lengths. The dimensions for the unit meshes varied from 5 nm to 10 nm when the meshes were on the or close to the structures. Maxwell's equations were solved with time steps of 0.0124088 fs (femtoseconds) over 1000 fs for each nanoantenna-MIM waveguide case. The following boundary conditions were used everywhere inside the simulation region, except for the simulation region boundaries:

$$\hat{a}_{21} \times [\vec{E}_2(t) - \vec{E}_1(t)] = 0$$

$$\hat{a}_{21} \times [\vec{H}_2(t) - \vec{H}_1(t)] = \vec{J}_s$$

$$\hat{a}_{21} \bullet [\vec{D}_2(t) - \vec{D}_1(t)] = \rho(t)$$

$$\hat{a}_{21} \bullet [\vec{B}_2(t) - \vec{B}_1(t)] = 0$$

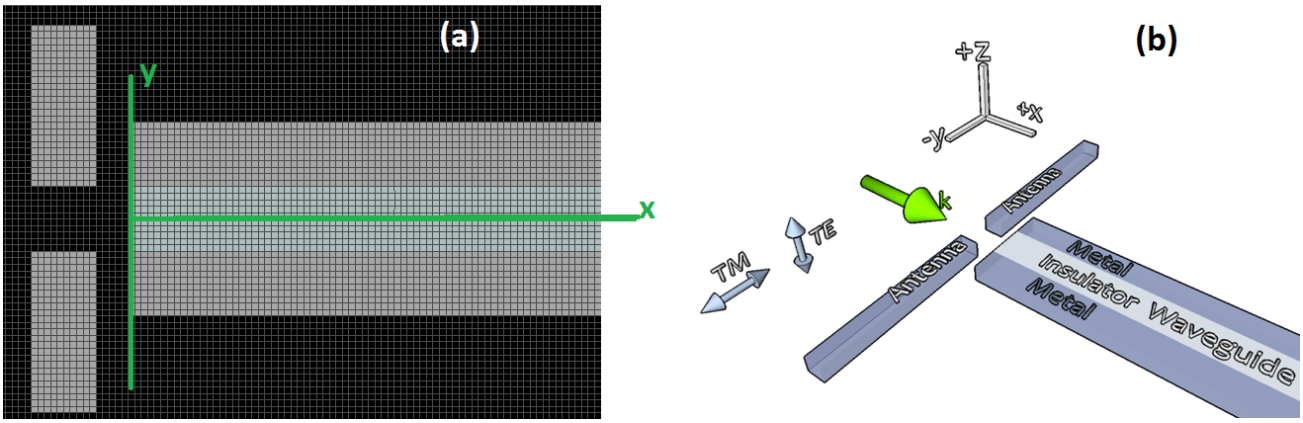

Figure 2. (a) Origin of the waveguide is shown as the intersection of x and y axes. (b) Structure of the waveguide combined with the dipole antenna has been shown with the orientations of transverse electric and transverse magnetic polarizations.

3. RESULTS AND ANALYSIS

In order to characterize the antenna-waveguide system, the effects of variation in each dimension (i.e. antenna arm length, antenna arm width, antenna-waveguide separation) on the waveguide response has been discussed below.

3.1 Mode field profile enhancement

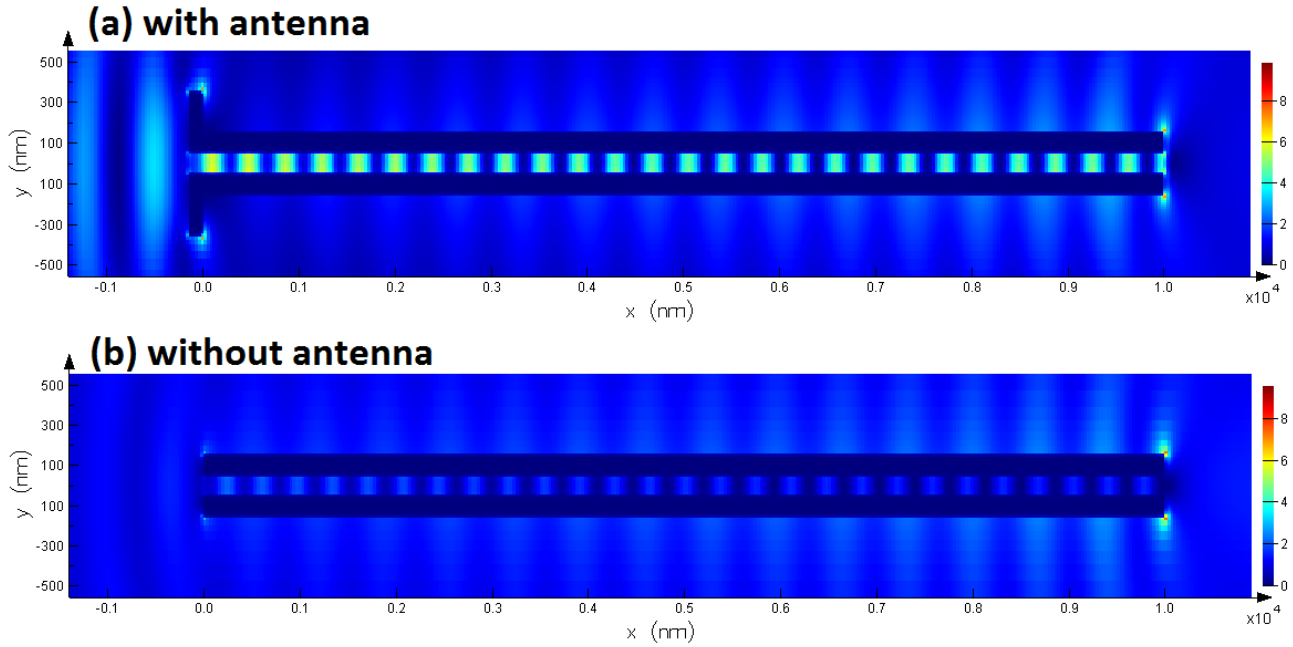

Figure 3. E field intensity profile in the steady state has been shown for (a) 300nm-arm-length antenna/waveguide system and (b) for the bare MIM reference. The color bars show the field normalized with respect to incident vacuum E-field intensity. (Free space incident wavelength λ = 1375 nm, TM polarization)

The basic idea of the simulations is demonstrated in Fig. 3, where the E-field intensities are depicted to show propagating plasmonic modes. Fig. 3a and 3b were plotted to show the plasmonic signal enhancement due to the introduction of antennas to the inlet of the MIM. The signal enhancement is especially significant for the mode field intensities inside and at the outlet of the MIM waveguide, since the antenna is going to be shown to focus light with its near-field evanescent field, unlike in conventional microwave antennas. Conventional microwave antennas do not utilize the near-field emission, but instead their design is completely based on the far-field radiation patterns. Here, near-field of the dipole antennas is more important because of the antenna dimensions and for coupling purposes discussed in the following sections.

In Fig. 3b, the bare MIM reference that does not have the dipole antenna coupler has been shown. The metal claddings show zero signal intensity, since Maxwellian boundary conditions do not allow the existence of fields inside metals beyond a certain penetration depth (generally less than 14 nm for our simulations). The propagating fields inside the metal claddings for both Fig. 3a and 3b are the coupled plasmonic modes propagating along the two insulator-metal interfaces of the MIM. Fig. 3a shows the case of same MIM waveguide with the antenna. By introducing the antenna, plasmonic modes have been enhanced inside the MIM and at the waveguide outlet. For the case in Fig. 3, the antenna-MIM system's signal at x=10 μm and y = 0 (MIM outlet, center of the core) is enhanced about 71.3 times that of the reference MIM.

This behavior is not only limited to 10 μm-long MIM waveguides. The simulations for 40 μm and longer waveguides with the same antenna (not shown) indicate that the signal intensity at 40 μm is not below a third of the signal intensity at 10 μm. The main loss, as discussed in the following figures, is due to the coupling loss which by far exceeds the material loss and signal dispersion. The focus of this study has thus been the mechanisms that facilitate and prevent MIM plasmonic mode coupling.

3.2 Waveguide response for increasing antenna-waveguide separation

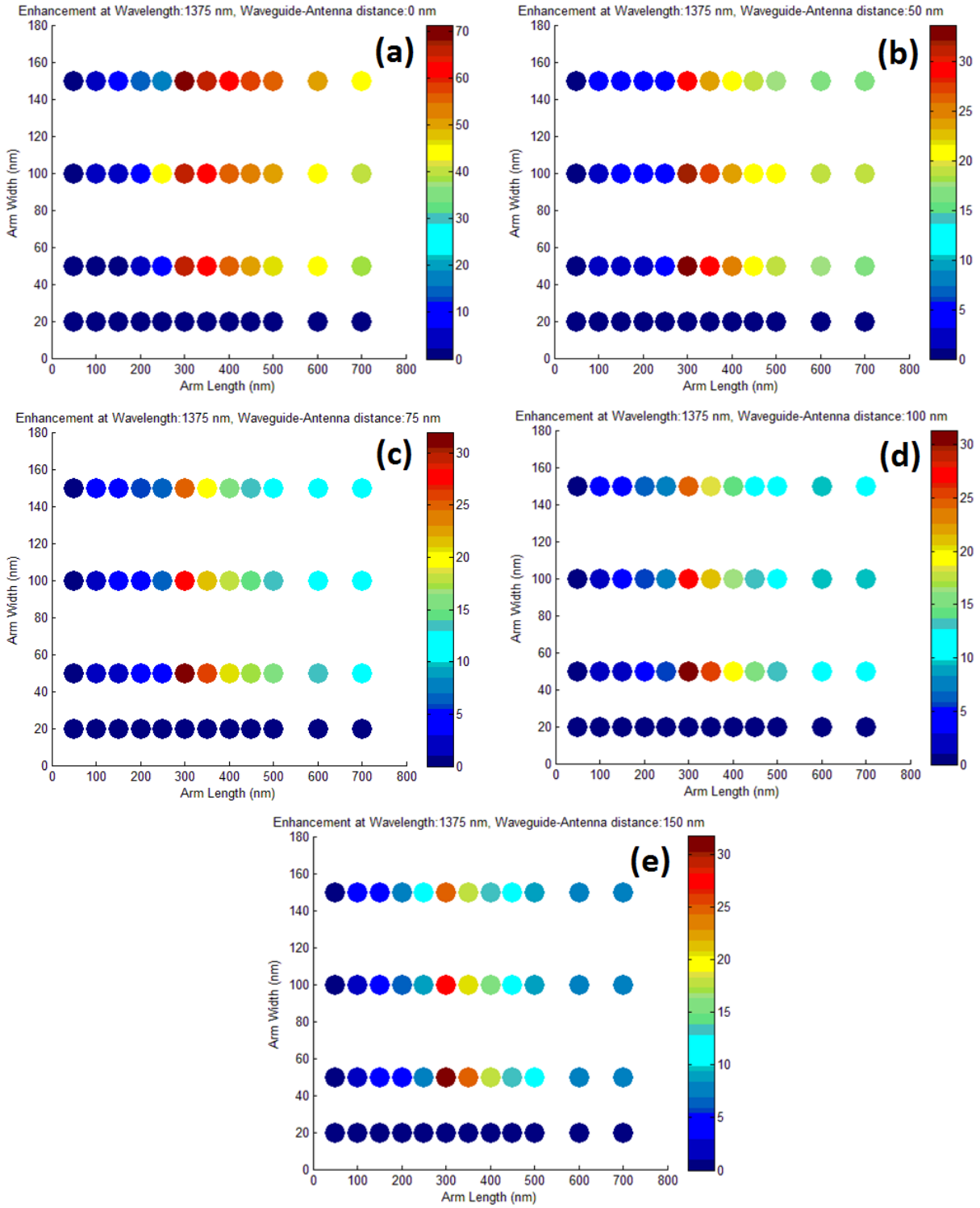

Figure 4. Enhancement factor of E-field at the outlet (at x = 10μm, y = 0) of the insulator core, as a function antenna arm length and width, for TM wave excitation at free space λ = 1375 nm.

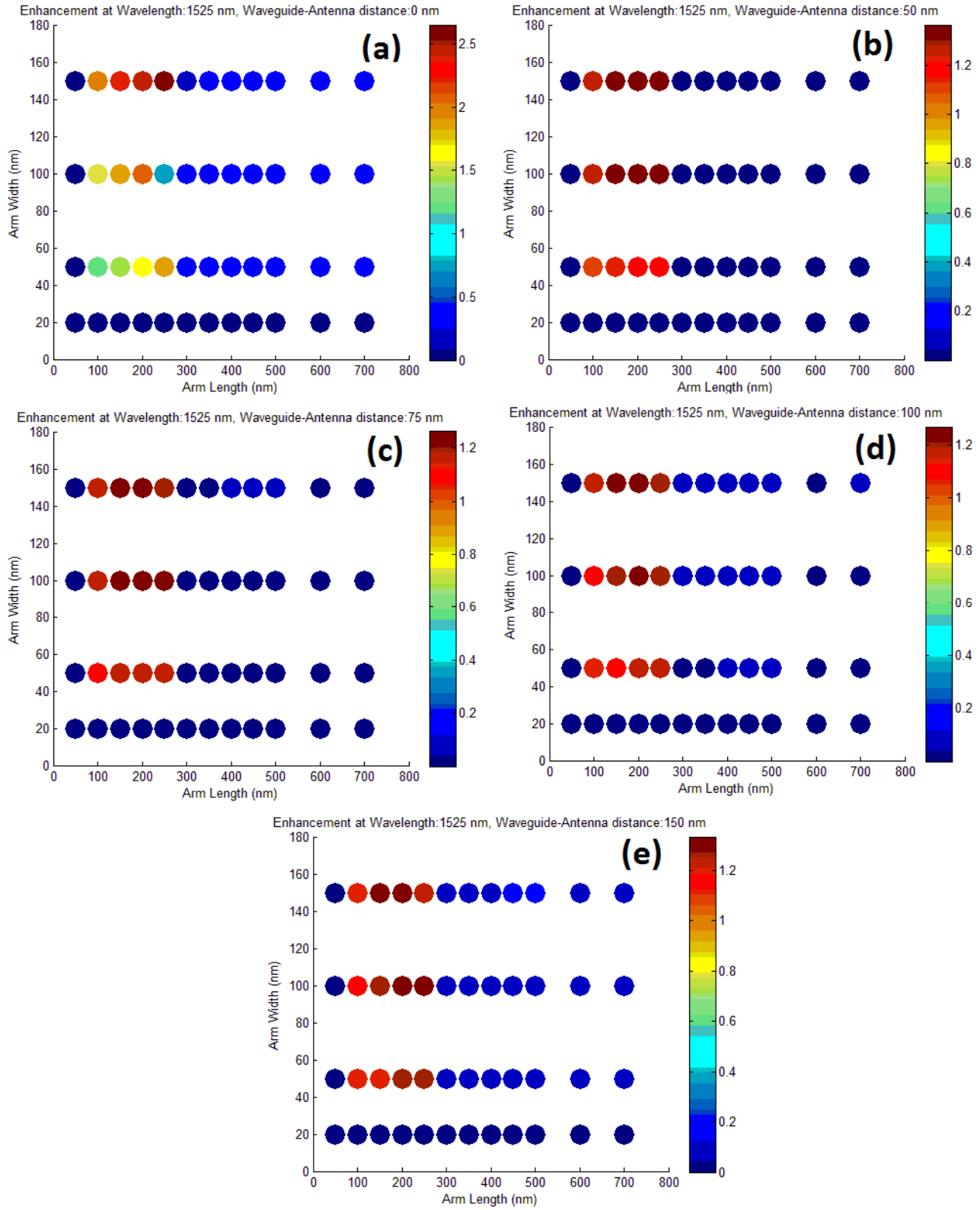

Figure 5. Same as in Fig.4 except that excitation is at 1525 nm. Fig.5(a) to 5(e) depict enhancements for different antenna-MIM distances.

Antenna-waveguide separation is the distance between the closest sides of the MIM waveguide and the antenna arms. The effect of a change in this distance is important for the explanation of the enhancement mechanisms of the electric field at the outlet of the insulator. Fig. 4 shows a part of the set of simulation results for TM wave excitation at λ = 1375 nm. Fig.4a to Fig.4e show the enhancement of the E-field intensity at the outlet of the insulator (x = 10 micron, y=0. at the middle of the insulator core) with respect to the reference MIM waveguide (enh = $|E_{w/antenna}|^2/|E_{(w/o)antenna}|^2$). Color bars show the enhancement factors, where maximum field intensity enhancement reaches 71.27x times that of the reference intensity. Fig5 shows a part of the simulation results for TM wave excitation at λ = 1525 nm, every other parameter set being the same as in Fig. 4. Waveguide response in different wavelengths (as in Figures 4 and 5) show that the antenna resonance covers λ = 1375 nm but not 1525 nm. There is still however, signal enhancement at the wavelength of 1525 nm.

In order to characterize the antenna-waveguide system, the waveguide response and enhancements have been investigated for increasing antenna-waveguide separations, ranging from 0 nm (connected structures), 50, 75, 100 nm and 150 nm. In Fig. 4a, i.e. when the antenna is connected to the MIM, the signal enhancement reaches maximum compared with other waveguide-antenna distances. For antenna arm lengths ranging from 300 nm to 700 nm and antenna arm widths ranging from 50 nm to 150 nm, enhancements are significant for each antenna-waveguide separation. The antenna's enhancement of the signal at the waveguide outlet gradually decreases as the separation increases as in Fig. 4a to Fig.4e. In particular, even 50 nm spacing between the waveguide and antenna is sufficient to halve all the enhancements. Thus, one of the most important results of the simulations in this section is that connected structures exhibit much stronger signal enhancements, with respect to bare MIM waveguides.

Another important result of these simulations as plotted in Fig. 3 is that there is a range of antenna dimensions that support enhancements greater than 40. In Fig. 3a, this region corresponds to the range arm length within [250, 700] nm and arm width within [50, 150]. While increasing antenna-waveguide spacing significantly reduces most of the wavelengths, there is more tolerance in antenna dimensions. Thus, fabrication tolerances in ion beam or electron beam lithography can be supported while still achieving more than 40 times enhancement.

The resonances of the antenna are coupled with the waveguide dimensions. MIM waveguide also acts as an antenna by itself, and it is possible to model the antenna coupler and the waveguide as two coupled antennas. In our study however, we preferred to vary the dipole antenna dimensions only and keep the waveguide dimensions constant for (i) the sake of simplicity, (ii) MIM waveguide length can be extended to beyond 50 μm, while signal intensity is still within a few dB of the initially coupled intensity (For such a case, coupled antenna analysis becomes less relevant.). (iii) MIM waveguide dimensions need to be kept below 400 nm in width in order to achieve high integration densities in parallel and for being competitive with respect to silicon-on-insulator or rib waveguides.

Even if the widths of the MIM waveguide claddings have been set to 100 nm, these dimensions can safely be reduced down to a few penetration depths (penetration depth ~ 14nm). This shows that there is still significant room for miniaturization and higher density integration of plasmonic MIM interconnects. In our analysis however, we avoided miniaturizing down below 100 nm widths for MIM waveguide, since fabrications requirements would then start becoming prohibitively stringent.

The enhancement regions in Fig. 4a to 4e are different than those in Fig. 3a to 3e. The enhancement region in Fig. 4 generally ranges for arm lengths being within [100, 250] nm and for arm widths being within [50, 150] nm, while the enhancement region of Fig. 3 requires longer antenna arm lengths. This is because of the coupled nature of the MIM waveguide and the antenna. When the antenna and the waveguide are not connected, the coupled nature becomes a damping factor due to Fabry-Perot resonances between the antenna and the MIM waveguide's input facet. When the antenna and the waveguide system are connected, the Fabry-Perot resonances are avoided and a much stronger coupling has been observed.

The near-field radiation pattern of the antenna can initiate a more intense plasmonic mode field inside the waveguide, when the overlap integral of the mode profile and the antenna radiation pattern is larger. For maximizing this overlap integral, it is necessary to tune to the antenna resonance wavelength and radiation profile for the MIM and keep the waveguide and antenna as close as possible.

3.3 Waveguide response for increasing antenna arm length

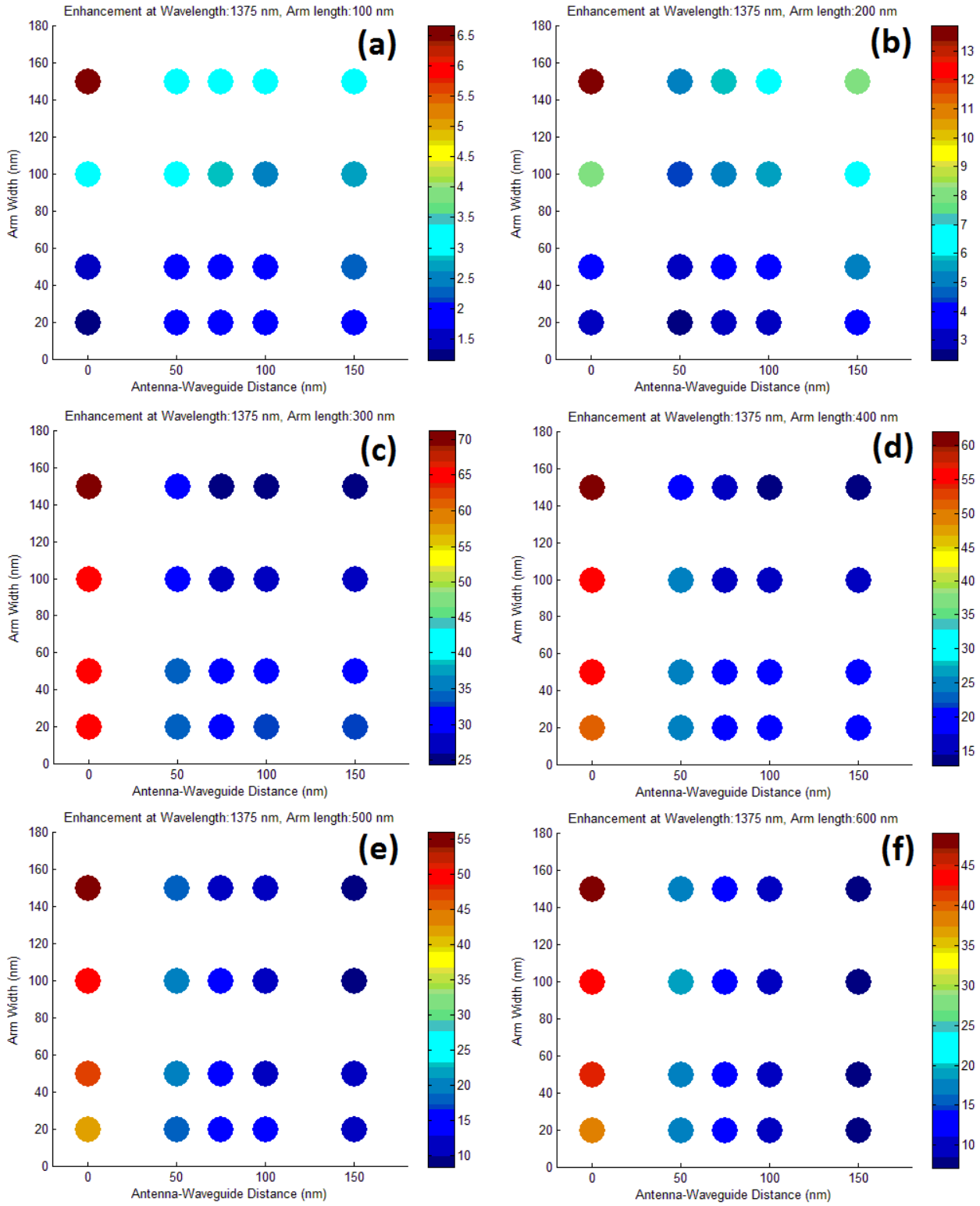

Figure 6. Structure of the waveguide combined with the dipole antenna has been shown with the orientations of transverse electric and transverse magnetic polarizations.

As stated at the end of the previous section, the antenna length needs to be tuned for achieving maximum coupling. For this purpose, the waveguide response as a function of arm width and antenna-waveguide distance has been analyzed and plotted in Fig. 6a to 6e, for different antenna lengths. Barnard et. al. showed that increasing antenna arm length introduces multiple resonance nodes along the antenna[22]. Though multiple spatial resonances along the antenna can be exploited for coupling purposes, we chose to keep the antennas as small as possible for achieving highest integration density with compact coupling elements.

Fig. 6 shows that maximum signal enhancement is achieved when the antenna arm length is 300 nm (for each arm). By varying the antenna arm length from 50 nm to 300 nm, the mode field enhancement at the waveguide increases for every longer arm. As previously discussed, the most prominent enhancement in Fig.6 is observed when the antenna and waveguide are connected. By increasing antenna arm lengths, the highest enhancement is observed at 300 nm arm length. Antenna theory would predict two quarter wavelength antennas for dipole couplers ($\lambda/4 \sim 344$ nm), however the slight deviation from the antenna theory is due (i) utilization of the near-field localization of evanescent fields and (ii) antenna-MIM interaction perturbing resonances of the structures.

3.4 Waveguide response for increasing antenna arm width

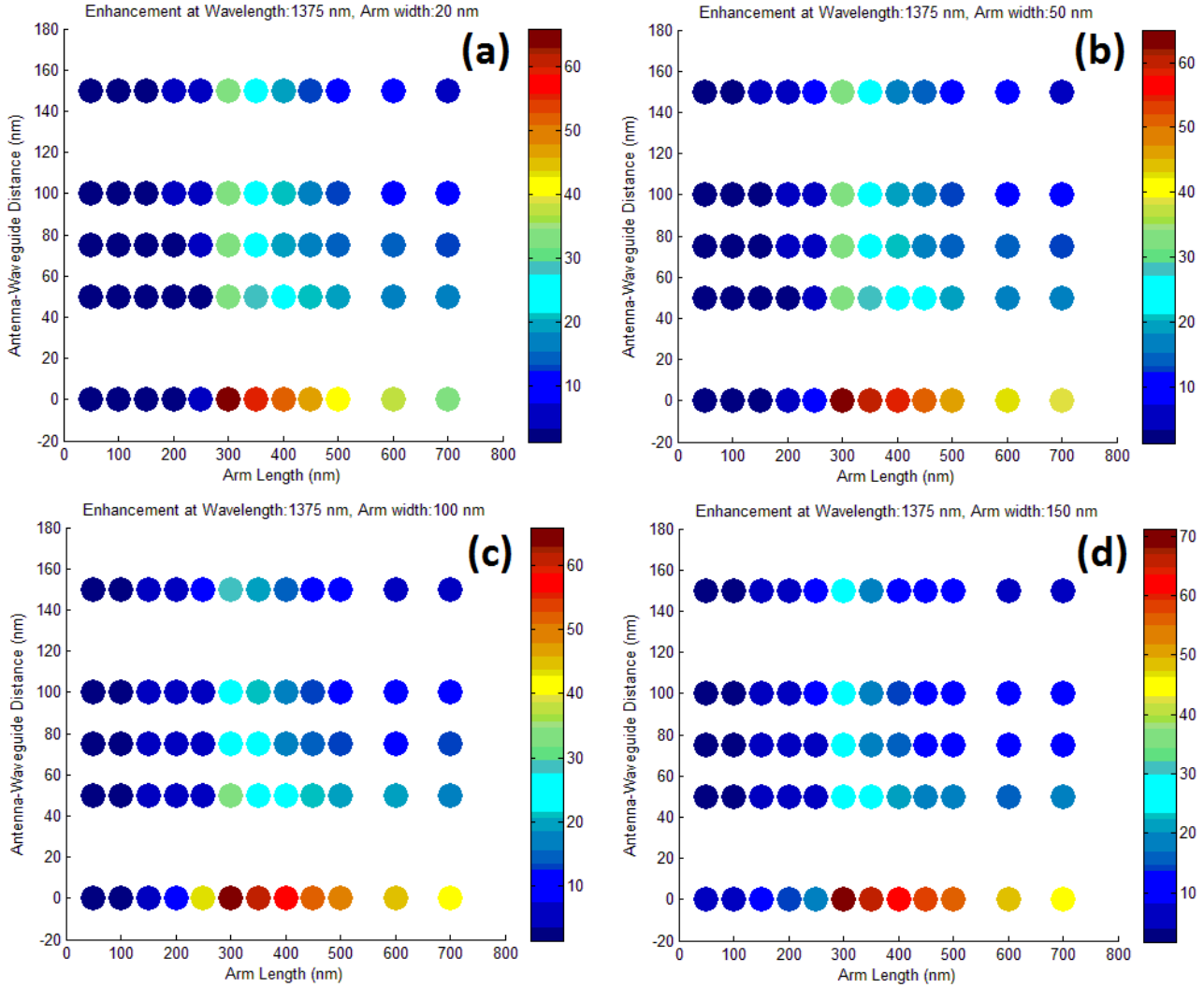

Figure 7. Signal enhancement factors at TM wave excitation at λ = 1375 nm as a function of different antenna arm lengths and antenna-waveguide separations. (a) to (d) were plotted for antenna arm widths 20, 50, 100, 150 nm respectively.

MIM waveguide response and signal enhancement to TM wave excitation at $\lambda = 1375$ nm has been shown in Fig. 7. The figures indicate the signal enhancement at the waveguide outlet as a function of different antenna arm-lengths and antenna-waveguide separations for arm widths ranging from 20 to 150 nm. The patterns generally show a peak at arm length of 300 nm for a connected antenna-waveguide system (i.e. antenna-waveguide distance is zero). The enhancement pattern essentially remains the same with similar enhancement factor values for increasing antenna arm widths up to 150 nm. This shows that antennas can be fabricated with 150 nm width without compromising much from the enhancement factor.

There are long tails to the peak and one tail ranges from arm length of 300 nm to 700 nm for connected cases (red dots). This wide shoulder is important in terms of allowing significant fabrication tolerances for the antenna arm length, since conventional lithographic techniques start failing generating feature sizes below 500 nm. There is yet another tail to the major peak, which range from antenna arm length of 300 to 500 nm, antenna-waveguide distance of 50 to 100 nm. Though this tail can only contain ~25 times signal enhancement (turquoise dots), fabrication imperfections (side wall roughness or tolerances in antenna geometry) might dictate the utilization of this enhancement region.

4. CONCLUSION

By introducing nanoantenna couplers, the signal output of the MIM interconnects can be enhanced significantly (upto more than 70 times) while the coupler space is reduced with respect to tapered coupling architectures. Enhancing the signal is important for integration of the MIM interconnects with CMOS compatible nanoscale photodetector elements (i.e. Ge-on-Si photodetectors) for converting plasmonic signals to electrical photocurrent. Finite-difference time domain (FDTD) simulations of antenna-waveguide structures for transverse electric (TE) and transverse magnetic (TM) incident plane waves were done for free space $\lambda = 1300$ to 1600 nm. Antenna width, length, and antenna-MIM separation distance are varied systematically. The main loss, as identified in the text, is because of coupling, which by far exceeds the material absorption and signal dispersion. The focus of this study has been the mechanisms that facilitate or prevent MIM plasmonic mode coupling.

For antenna arm lengths within [300, 700] nm and antenna arm widths within [50, 150] nm, enhancements are significant for each antenna-waveguide separation. The antenna's enhancement of the signal at the waveguide outlet gradually decreases as the separation increases. Signal is damped in disconnected antenna-MIM systems due to Fabry-Perot resonances between the antenna and the MIM waveguide's input facet. When the antenna and the waveguide system are connected, the Fabry-Perot resonances are avoided and a much stronger coupling has been observed. While increasing antenna-waveguide spacing significantly reduces enhancement, there is more tolerance in antenna dimensions. Thus, fabrication tolerances in ion beam or electron beam lithography can be supported while still achieving more than 40 times enhancement.

The near-field radiation pattern of the antenna can initiate a more intense plasmonic mode field inside the waveguide, when the overlap integral of the mode profile and the antenna radiation pattern is larger. For maximizing this overlap integral, it is necessary to tune to the antenna resonance wavelength and radiation profile for the MIM and keep the waveguide and antenna as close as possible. For $\lambda = 1375$ nm, the highest enhancement is observed at 300 nm arm length. For the optimum case, there are slight deviations from a quarter wavelength antenna as predicted by the antenna theory, due to the utilization of the near-field localization and antenna-MIM interaction perturbing resonances of the structures.

REFERENCES

[1] D. A. B. Miller, "Physical Reasons for Optical Interconnection," Special Issue on Smart Pixels, Int'l J. Optoelectronics **11** (3), 155-168 (1997).

[2] G. Moore, "Cramming more components onto integrated circuits", Electronics, 38, 8, April 19, 1965

[3] Snyder, A. W. and Love, J. D., [Optical Waveguide Theory], Kluwer Academic Publushers Group, Norwell, Massachusetts, (2000).

[4] J. Dostalek, H. Vaisocherova, J. Homola, "Multichannel surface plasmon resonance biosensor with wavelength division multiplexing", Sensors and Actuators B 108 (2005) 758–764

[5] P. Berini, Bulk and surface sensitivities of surface plasmon waveguides, New Journal of Physics **10** (2008) 105010

[6] K.M. Evenson, D.A. Jennings, K.R. Leopold, and L.R. Zink, "Tunable Far Infrared Spectroscopy", Appl. Phys. Lett. 44 (6). 15 March 1984

[7] M. T. Hill, M. Marell, E. S. P. Leong, et. al., "Lasing in metal-insulator-metal sub-wavelength plasmonic waveguides", Optics Express, **17**, 13, pp. 11107-11112 (2009)

[8] Zongfu Yu, Georgios Veronis, Shanhui Fan, M. L. Brongersma, "Gain-induced switching in metal-dielectric-metal plasmonic waveguides", Applied Physics Letters 92, 041117 (2008)

[9] Dionne, J. et. al., "Silicon-Based Plasmonics for On-Chip Photonics", IEEE Journal of Selected Topics in Quantum Electronics, Vol. 16, No. 1, pp. 295- 306, January/February 2010

[10] Dionne, J. et. al., "Plasmon slot waveguides: Towards chip-scale propagation with subwavelength-scale localization", Physical Review B 73, 035407 (2006)

[11] Veronis, G.; Fan, S.; "Modes of Subwavelength Plasmonic Slot Waveguides", Journal of Lightwave Technology, Vol. 25, No. 9, Sept. 2007 2511

[12] S. E. Kocabas, G. Veronis, D. A. B. Miller, and S. H. Fan, "Modal Analysis and Coupling in Metal-Insulator-Metal Waveguides," Phys. Rev. B **79**, 035120 (2009)

[13] D. K. Gramotnev, S. I Bozhevolnyi, Nature Photonics, Vol. 4, Feb. 2010, 83

[14] S. I Bozhevolnyi, Nature Photonics, Vol. 440, 23 March 2006, 508

[15] Bozhevolnyi, S. I, ed., [Plasmonic Nanoguides and Nanocircuits], Pan Stanford Publishing, Hackensack, NJ (2008)

[16] R. F. Oulton, V. J. Sorger, D. A. Genov, D. F. P. Pile & X. Zhang, "A hybrid plasmonic waveguide for subwavelength confinement and long-range propagation", Nature Photonics 2, 496 - 500 (2008)

[17] R. Zia, M. D. Selker, P. B. Catrysse, and Mark L. Brongersma, JOSA A, 21, 12, 2442 – 2446

[18] P. Ginzburg, David Arbel, and Meir Orenstein, "Gap Plasmon polariton structure for efficient microscale-to-nanoscale interfacing", Optics Letters, 31, 22, (2006)

[19] S. Lardenois et. al., "Low-loss submicrometer silicon-on-insulator rib waveguides and corner mirrors", Optics Letters, 28, 13, 1150-1152 (2003)

[20] Palik, E. D., [Handbook of Optical Constants], Academic Press, 1998

[21] Lumerical FDTD Solutions Inc., Suite 201 - 1290 Homer Street Vancouver, British Columbia, Canada

[22] E. Barnard, J. White, A. Chandran, and M. Brongersma, "Spectral properties of plasmonic resonator antennas," Opt. Express 16, 16529-16537 (2008).